

Activated Dissociation of H₂ on Cu(001): The Role of Quantum Tunneling

Xiaofan Yu^{1,2#}, Yangwu Tong^{1,2#}, and Yong Yang^{1,2*}

1. *Key Lab of Photovoltaic and Energy Conservation Materials, Institute of Solid State Physics, HFIPS, Chinese Academy of Sciences, Hefei 230031, China.*
2. *Science Island Branch of Graduate School, University of Science and Technology of China, Hefei 230026, China.*

ABSTRACT:

The activation and dissociation of H₂ molecules on Cu(001) surface is studied theoretically. The activation barrier for the dissociation of H₂ on Cu(001) is determined by first-principles calculations to be ~ 0.59 eV in height. Electron transfer from the substrate Cu to H₂ plays a key role in the activation, breaking of the H-H bond and the formation of the Cu-H bonds. The competition of H-H and Cu-H bonds may be described by the overlap of the wave functions of the outermost valence electrons. Using the transfer matrix method, we are able to study the role of quantum tunneling in the dissociation process, which is found to be significant at room temperature and below. At given temperatures, the tunneling contributions from the translational and vibrational motions of H₂ are quantified for the dissociation process. Within a wide range of temperatures, the effects of quantum tunneling on the effective barriers of dissociation and the rate constants are revealed. The deduced energetic parameters associated with thermal equilibrium and non-equilibrium (molecular beam) conditions are comparable with experimental data. In the low-temperature region, crossover from classical to quantum regime is identified.

[#]These authors contribute equally to this work.

*Corresponding author: yyanglab@issp.ac.cn

1. Introduction

As a clean energy source, hydrogen mainly exists in the form of molecules in nature. Materials involving metal elements are commonly utilized as catalysts for hydrogen production and storage to harvesting hydrogen based energy [1-3]. The elementary dynamics (e.g., adsorption and diffusion) of hydrogen on transition metal surfaces are closely related to some important physical and chemical processes such as crystal growth, hydrogen embrittlement in metals, surface corrosion, and technological applications like radiation protection in fusion reactor reactions, electrode reactions in fuel cells, and surface catalysis [4-19]. When H_2 molecules approach a metal surface, depending on the energetics, they may exist in the molecular form, or the dissociative form with the H atoms attached separately on the metal surface. The key factor determining the energetics is the energy path in particular the energy barrier associated with the dissociation process, which is referred to as the dissociation barrier hereafter. It is found that the dissociation barriers of hydrogen molecules on different metal surfaces are different. For instance, on the surfaces of Pt and Rh, the adsorbed H_2 molecules will spontaneously decompose into H atoms [20-22]. By contrast, on the surface of Cu and Ag [23], the adsorbed H_2 molecules do not spontaneously decompose into H atoms, and the dissociation process requires additional energy consumption, which is usually referred to as an activated process. In the spontaneous process, the related energy barrier $E_b = 0$ whereas $E_b > 0$ in the activated process. The dissociation barriers of hydrogen on different crystallographic planes are also quite different. The existence of an activation barrier is commonly believed to be due to the full occupation of d orbitals which induces Pauli repulsion when molecules and surfaces come into contact [24, 25]. Consequently, dissociation of H_2 on the metal surface with fully occupied d orbitals tends to be an activated process ($E_b > 0$), while dissociation on the metal surface with partially occupied d orbitals is more likely to be a spontaneous process ($E_b = 0$). There have been many experimental reports [6, 8, 10, 14, 15] on the adsorption, dissociation and diffusion processes of hydrogen on different metal surfaces. For example, nozzle beam experiment in combination with sticking coefficient measurements for monoenergetic

molecular beams as a function of energy and angle of incidence were carried out to study the adsorption/desorption kinetics of H_2 on Cu surfaces [6]. Using thermal desorption in combination with work function and low electron diffraction (LEED) measurements, the H/Pd(100) system has been studied to determine the adsorption state and adsorption energy [8]. Molecular beam techniques were utilized to control the incident kinetic energy and incident angle of H_2 molecules to explore in detail the nature of the dissociation barriers on Cu [10]. As a typical prototype system for the activated reactions of H_2 with metal surfaces, H_2 /Cu has been the subject of many theoretical investigations, focusing primarily on the dissociation and sticking probabilities [26-38], and the thermal desorption spectra [39], which are directly related to the energy pathway governing the dissociation/desorption processes. Based on the potential energy surface (PES) constructed within the Born-Oppenheimer approximation, six-dimensional quantum dynamics calculations have been carried out to study the activated dissociation of H_2 on Cu(100) [26-31], with focus on the role of vibrational and rotational states of H_2 , as well as the coupling of both degrees of freedom [27-30]. In recent years, special attention is paid to the development of chemically accurate PES for the interactions between H_2 and Cu and other metal surfaces [32-38]. Notable progress in this field includes, for instance, the implementation of semi-empirical specific reaction parameter (SRP) approach to density functional theory (DFT) [32-37], and the recently developed machine learning based PES [38].

Compared to the other elements, hydrogen has a smaller mass and therefore significant nuclear quantum effects are expected in its dynamical process [40-43]. In recent years, the important role of atomic quantum tunneling plays in the reaction rates and selectivity of chemical processes involving small molecules has been increasingly reported [44, 45]. Despite the enormous number of experimental and theoretical investigations, little is known about the role quantum tunneling plays in the activated dissociation process of H_2 on metal surfaces. In the present work, we revisit this topic studying the activation and dissociation of H_2 molecules on Cu(001). The effects of quantum tunneling are investigated based on first-principles

calculations combined with the transfer matrix method. During the activation process of H_2 on $\text{Cu}(001)$, it is shown that the charge transfer between the Cu surface and the H_2 molecule is the key for the breaking of H-H bond and the formation of Cu-H bonds. The probability of dissociation and the corresponding rate constants due to the translational (H_2 tunneling as a whole unit) and vibrational motions of H_2 molecules are quantitatively evaluated. The obtained activation barrier and the threshold kinetic energy for detectable dissociation events are in agreement with experimental observations. The effective dissociation barrier is evaluated as a function of temperature, whose magnitude is found to be significantly reduced owing to the quantum tunneling of H atoms. For the dissociation of hydrogen isotopes H_2 and D_2 , the crossover from the high-temperature classical dynamics to low-temperature quantum dynamics is recognized.

This paper is organized as follows. Following the introductory part, Section 2 presents the technical details of first-principles calculations and the transfer matrix (TM) method employed in this study. In Section 3, the results on the energy path of the activated dissociation of H_2 on $\text{Cu}(001)$, the role of charge transfer and wave function overlap, and the role of quantum tunneling in shaping the kinetic process are presented and compared with experiments. Section 4 summarizes the main conclusions.

2. Methods

2.1 Details of First-principles Calculations

The Vienna *ab initio* simulation package (VASP) [46, 47] based on density functional theory (DFT) is employed for the first-principles calculations. The Perdew-Burke-Ernzerhof (PBE) type functional within the generalized gradient approximation (GGA) [48, 49] is used to describe the exchange-correlation terms of electrons, in combination with the PAW potentials [50, 51] to describe the electron-ion interactions. The energy cutoff for plane wave basis sets is 600 eV. The initial atomic configurations are constructed with the aid of VESTA [52], in which the $\text{Cu}(001)$ surface is modeled by a six-layer $p(3 \times 3)$ supercell, repeating periodically

along the xy plane with a vacuum layer of about 15 Å along the z direction. In all the calculations, the Cu atoms in the bottom three layers are fixed and the atoms in the upper layers are relaxed. We employ a dipole correction for the total energy to eliminate the artificial dipole-dipole interaction caused by the upper and lower asymmetric slab surfaces. A $4 \times 4 \times 1$ Monkhorst-Pack k -mesh [53] is generated for sampling the Brillouin zone (BZ) in performing structural relaxation and total energy calculations. The vibrational properties of the relaxed structures are analyzed using density functional perturbation theory (DFPT) [54].

2.2 The Transfer Matrix Method

The probability of a quantum particle passing through a potential barrier of arbitrary shape can be obtained using the transfer matrix (TM) method. By numerically slicing an arbitrarily shaped potential, it is transformed into a stack of multiple rectangular potential barriers (potential wells) [43]. The transmission of a particle through each rectangular potential barrier (potential well) can be represented by a matrix of coefficients that describe the transmitted and reflected amplitudes of the wave function. Multiplying the coefficient matrices in turn one is able to obtain a transition matrix representing the transition relationship between the initial and the final state. For the transmission across a potential $V(x)$, the incoming and outgoing amplitudes $(A_L, B_L; A_R, B_R)$ of the wave functions can be related to each other as follows [43]:

$$\begin{pmatrix} A_R \\ B_R \end{pmatrix} = M \begin{pmatrix} A_L \\ B_L \end{pmatrix} \quad (1)$$

where $M \equiv \begin{pmatrix} m_{11} & m_{12} \\ m_{21} & m_{22} \end{pmatrix}$ is the transfer matrix. In a system which preserves the time-reversal symmetry, the determinant $|M| = 1$, and the transmission coefficient is calculated by $T_r(E) = \frac{1}{|m_{22}|^2}$.

The advantage of the TM method is that the obtained transmission probabilities are numerically accurate with comparison to that calculated by the Wentzel–Kramers–Brillouin (WKB) approximation [55]. For instance, when the incident energy of a classical particle is higher than the potential barrier, the probability of the particle

passing through the barrier is 1. For a quantum particle, due to the existence of quantum interference, even if the energy of the particle is greater than the barrier height, there may be a certain probability of reflection which makes the probability of passing through the potential barrier smaller than 1. The TM method deals with the transport of quantum particles in a given potential field in a unified manner, and fully takes into account quantum effects in the process of crossing a potential barrier.

3. Results & Discussion

3.1. Mechanistic analysis of the interaction between H₂ and Cu(001)

We begin by investigating the atomistic process of H₂ dissociation and dissociative adsorption on the Cu(001) surface. Shown in Fig. 1, are some typical configurations representing the dissociation process of a H₂ molecule which approaches the Cu(001) along the surface normal (*z*) direction. The orientation line of H-H bond is parallel to Cu(001), the midpoint of H-H bond is right above one of the bridge sites of Cu(001) with the projection of H-H bond perpendicular to the surface Cu-Cu bond. Such an initial configuration gives rise to the largest possibility of dissociation [17, 25]. It is found by our calculations that, when the distance between the H₂ molecule and the Cu (001) surface decreases to a critical value ($z_c = 0.930 \text{ \AA}$), the covalent bond in the H₂ molecule is broken and decomposes into two adsorbed H atoms on the Cu(001). The corresponding energy pathway of this process is shown in Fig. 2(a). Before the onset of the dissociation, the energy of the system is continuously rising with decreasing H₂-Cu(001) distance. At the critical point of H-H bond breaking, there is a sudden change and the energy of the system drops abruptly. Accordingly, the energy drop (from configuration C to D) in this process corresponds to the desorption barrier of chemically adsorbed H on Cu(001). The height of the barrier ($E_b \sim 0.586 \text{ eV}$) is in good agreement with previous works ($E_b \sim 0.58 \text{ eV}$) [17, 36, 56] at the GGA level and is lower than the barrier height ($E_b \sim 0.74 \text{ eV}$) calculated using the SRP-DFT method [33, 35, 36]. Experimentally, temperature programmed desorption (TPD) is commonly employed to measure the desorption barrier and desorption rate of H₂ on the Cu(001) surface [15], which can be numerically

simulated based on DFT calculations in combination with kinetics analysis[39]. To understand the bond breaking from the level of electron dynamics, we study the charge transfer between H₂ molecule and the substrate using the Bader analysis [57]. As seen from Fig. 2(b), when a H₂ molecule gradually approaches the Cu(001), electrons from the underlying Cu substrate are gradually transferred to the two H atoms. The distance between the hydrogen molecule and the surface of Cu(001) is $Z_{\text{H}_2\text{-Cu(001)}} \approx 0.930 \text{ \AA}$, corresponding to a decrease of height $|Z_0 - Z| \approx 2.576 \text{ \AA}$. As shown in Fig. 2(a), the total energy of the system drops steeply at this position. Meanwhile, a sharp increasing of the charge transfer to H atoms is observed (Fig. 2(b)). The abrupt change in both the total energy and the number of transferred electrons indicates that the dissociation of hydrogen molecules at the critical point may be an ultrafast process.

To get more insights into the dynamical process associated with charge transfer, we have calculated the charge density differences for a number of typical adsorption configurations, including the initial molecular state, the intermediate and transition states of dissociation, and the final fully dissociated state on Cu(001). Practically, the charge density difference ($\Delta\rho$) of a given configuration is obtained by subtracting the charge density of substrate and two individual H atoms from the total charge density of the adsorption system. The formula is as follows:

$$\Delta\rho = \rho[\text{H}_2/\text{Cu(001)}] - \rho[\text{H}_1] - \rho[\text{H}_2] - \rho[\text{Cu(001)}], \quad (2)$$

where $\rho[\text{H}_2/\text{Cu(001)}]$ is the charge density of the system of H₂/Cu(001), $\rho[\text{H}_1]$ and $\rho[\text{H}_2]$ denotes respectively the charge density of the two H atoms, $\rho[\text{H}_2/\text{Cu(001)}]$ is the total charge density of the adsorption system.

The isosurfaces of charge density differences are shown in Fig. 3. When the H₂ molecule is far away from the Cu(001) surface, there is no charge transfer between H₂ and the substrate. Instead, one sees mainly the charge difference with positive values in-between the two H atoms (Fig. 3(a)), a clear evidence of the formation of H-H covalent bond. As the distance between H₂ and Cu(001) decreases, the electrons from substrate Cu start to transfer to the H atoms. The closer they are, the larger amount of charge transfer is found. When the H₂-Cu(001) distance is $z = 0.749 \text{ \AA}$, the two H

atoms are separated from each other and the H-H covalent bond is broken. The H atoms are located between four nearest neighboring Cu atoms and exchange charges with them. The H atoms gain electrons and the Cu atoms lose electrons. The electrons gather around the H atoms and indicate some characteristics of ionic bond between H and Cu atoms. Figure 4 shows the two-dimensional (2D) contours of charge distribution, which is sliced along the surface normal plane through the centers of the two H atoms. When the H₂-Cu(001) distance $z = 0.592 \text{ \AA}$, the covalent bond is completely broken. It is worth noting that the H-H bond is very weak at $z = 0.930 \text{ \AA}$, but it is still not broken, which can be regarded as the critical intermediate state. The breaking of the H-H bond is observed to be instantaneous when H₂-Cu(001) distance exceeds the critical value ($z_c = 0.930 \text{ \AA}$). Figure 5 shows the variation of 2D charge distribution between the one of the H (the other one is geometrically equivalent) and the nearest neighboring Cu atoms. At the initial distance $z = 2.460 \text{ \AA}$, the H-Cu bond does not exist. As the distance between the H₂ molecule and the Cu(001) surface decreases, the H-Cu bond is gradually formed and strengthened. Finally, the H atoms form H-Cu bonds with the nearest neighboring Cu atoms. The charge contours clearly demonstrate the formation of H-Cu bonds when a H₂ molecule approaches the Cu(001) surface.

From the analysis above, one may come to realize that the adsorption and dissociation of H₂ molecules on Cu(001) is essentially the competition between H-H and H-Cu bonds. Regarding the forces governing this process, the nuclear (ion core) – electron interactions are attractive, and the nuclear (ion core) – nuclear (ion core), electron – electron interactions are repulsive. The balance between the attractive and repulsive forces leads to the formation of chemical bonds. The strength of attraction is largely related to the extent of overlap of electron wave functions, which can be quantitatively described by the overlap integral. As a result, the strength of attraction and bonding between two atoms are largely determined by the overlap of wave functions of electrons that participate in the bond formation. For a given atom in molecular form, when the attraction from a foreign species of atom is larger than the one it bonded with, breaking of the old bond and formation of a new bond is therefore

expected. In our case, it is possible to understand the dissociation process of H₂ on Cu(001) by comparing the overlap integrals between the 1s orbitals of H atoms and the 4s orbitals of Cu, i.e., 1s(H)-1s(H) versus 1s(H)-4s(Cu).

To evaluate the overlap integral, the wave functions of the 1s orbital of H and the 4s orbital of Cu are needed. The wave function of the 1s orbital of H is readily obtained from textbook, while this is not the case for the 4s orbital of Cu. The electron shell arrangement of a Cu atom in the ground state is [Ar]3d¹⁰4s¹ with the *d* orbitals fully occupied. The outermost 4s electrons of Cu atoms can be regarded as the electrons of a hydrogen-like atom since the inner shell orbitals are all fully occupied. The wave function of the 1s orbital of H atom is [58]

$$\psi_{100}(r) = \left(\frac{1}{\pi}\right)^{1/2} \left(\frac{1}{a}\right)^{3/2} e^{-r/a}, \quad (3)$$

where the Bohr radius $a = \frac{4\pi\epsilon_0\hbar^2}{me^2} = 0.529 \text{ \AA}$, m is the electron mass, ϵ_0 is the vacuum permittivity, e is the charge of electron, \hbar is the reduced Planck constant, r is the distance between the electron and the nucleus. The ground-state energy of the hydrogen atom is $E_{1H} = -\left(\frac{m}{2\hbar^2} \left(\frac{e^2}{4\pi\epsilon_0}\right)^2\right) = -\frac{e^2}{4\pi\epsilon_0} \times \frac{1}{2a}$.

The wave function of the 4s orbital of a hydrogen-like atom is as follows [59]:

$$\psi_{400}(r) = \left(\frac{Z}{4a}\right)^{3/2} e^{-Zr/4a} \left(1 - \frac{3Zr}{4a} + \frac{Z^2r^2}{8a^2} - \frac{Z^3r^3}{192a^3}\right) \left(\frac{1}{\pi}\right)^{1/2} \quad (4)$$

where Z is the effective nuclear charge number. The corresponding eigenenergy of the 4s orbital of a hydrogen-like atom (with the Hamiltonian \hat{H}) with an effective nuclear charge number Z is

$$E_4 = \langle \psi_{400} | \hat{H} | \psi_{400} \rangle = -\frac{e^2}{4\pi\epsilon_0} \times \frac{1}{2a} \times \frac{Z^2}{4^2} \quad (5)$$

By definition, the eigenenergy E_4 is related to the first ionization energy (I_1) of Cu atoms as follows $I_1 = 0 - E_4 = \frac{e^2}{4\pi\epsilon_0} \times \frac{1}{2a} \times \frac{Z^2}{4^2} \equiv -E_{1H} \times \frac{Z^2}{4^2}$. Since $E_{1H} = -13.6 \text{ eV}$ and $I_1 = 7.72 \text{ eV}$ for Cu [60], it follows that $Z = 4 \times \sqrt{-\frac{I_1}{E_{1H}}} = 3.01$. The effective nuclear charge number Z includes the complex many-body effects of the nucleus-electron, electron-electron interactions.

The 1s-1s orbital overlap integral for H-H interactions is

$$I_{HH} = \iiint \psi_{100}(x, y, z) \psi_{100}(x, y - d, z) dx dy dz \quad (6)$$

The 4s-1s orbital overlap integral for Cu-H interactions is

$$I_{CuH} = \iiint \psi_{400}(x, y, z) \psi_{100}(x, y, z - h) dx dy dz \quad (7)$$

where d is the distance between the two H atoms under consideration, and h is the distance between H_2 and Cu(001).

Using the series of atomic configurations obtained by first-principles calculations when a H_2 molecule approaches the Cu(001), we are able to numerically calculate the overlap integrals (I_{HH} , I_{CuH}) as a function of the H-H distance (d_{H-H}). For calculation of I_{CuH} , the contributions from the first and second nearest neighboring Cu atoms are taken into account, which are denoted as $I_{1\ Cu-H}$, and $I_{2\ Cu-H}$, respectively. For each H atom, there are two first and second nearest surface Cu atoms. The overlap integral for H-Cu interactions is therefore $I_{CuH} = 4 \times (I_{1\ Cu-H} + I_{2\ Cu-H})$. The results are shown in Fig. 6. It can be seen from Fig. 6(a) that the overlap integrals of 1s-1s for H-H, and the 1s-4s for H-Cu orbitals are equal to each other at the configuration when $d_{H-H} \sim 1.63$ Å (labeled as Ic). This critical point indicates that the coexistence of H-H bond and the H-Cu bond. However, the configuration Ic is dynamically unstable. Shown in Fig. 6(b), is the calculated potential energy surface of the configurations at approximately the critical height ($z = z_c$), as a function the H-H separations. It can be inferred that the net force (the first derivative of energy E_0 with respect to d_{H-H}) acting on the configuration Ic is nonzero, which causes intrinsic instability and the elongation of H-H bond. This explains the abrupt change of the H-H bond length as well as the H_2 -Cu(001) distance upon the onset of bond breaking on Cu(001). The bond-breaking configuration arrives at a metastable configuration when the relative energy reaches a local minimum at $d_{H-H} \sim 3.71$ Å, at which the net forces acting on the H atoms are zero (labeled as configuration Ib).

3.2. Role of quantum tunneling in the dissociation processes

For a H_2 molecule incident on the Cu(001), the line joining the H-H bond can be parallel or perpendicular to Cu(001). Generally, the orientation of H-H bonds with respect to the Cu(001) surface can be described by an angle α , which belongs to the

range of $0 \leq \alpha \leq 90^\circ$. Previous studies based on the semi-empirical embedded-atom method (EAM) have shown that the barrier for H_2 dissociation on Cu(100) depends on the orientation angle [17]. Dissociation occurs more easily when the H-H axis is parallel to the surface. This is reasonable since when the H_2 molecule is close to the Cu(001), it has the largest contact with the surface and therefore the biggest chance of reaction and dissociation. Therefore, we only consider the case of $\alpha = 0$ here, for which the axis of the H-H bond is parallel to Cu(001). From the dynamical point of view, the dissociation of H_2 molecules on Cu(001) is mainly due to the contribution of two processes. The first process is the dissociation due to the translational motion of H_2 in the vertical direction. As shown in Fig. 7(a), a H_2 molecule approaches Cu(001) along the z direction by overcoming the potential barrier $U(z)$, and reaches the state of dissociation and chemisorption. The second process is the dissociation due to the stretching vibrations of H atoms in the horizontal direction (parallel to Cu(001)). As shown in Fig. 7(b), while approaching the Cu(001) along z direction, the lateral vibrations of each H atom provides an additional probability of breaking the H-H bond by overcoming the lateral potential barrier $U(x, y)$. This can be determined by standard DFT calculations. For a given temperature T , the dissociation probabilities of the two processes can be calculated separately, and the total dissociation probability is obtained by summing up the probabilities of the two processes. Unless otherwise stated, both H_2 molecules and single H atoms are treated as quantum particles to study the role of quantum tunneling. For the first process, the probability of dissociation is

$$P_{\perp}(T) = \int_0^{\infty} p(E, T) T_r(E) dE \cong \int_0^{E_m} p(E, T) T_r(E) dE, \quad (8)$$

where $p(E, T) = 2\pi(\frac{1}{\pi k_B T})^{3/2} \sqrt{E} e^{-E/k_B T}$ is the kinetic energy distribution function [61], which is suitable for the particles in thermal equilibrium systems where parabolic momentum-energy relation presents and scalar potentials dominate the interactions [43], T is the absolute temperature, E is the incident energy, k_B is the Boltzmann constant. The term $T_r(E)$ is the transmission probability of the H_2 molecule as whole unit across the potential barrier $U(z)$ (Fig. 7(a)) at a certain energy E , which is calculated by transfer matrix (TM) method. In practice, an upper bound

(E_m) is set for evaluation of the integral, which ensures the numerical results to converge to desired precision.

For the second process, the probability of dissociation is

$$P_{//}(T) = \frac{1}{L} \int_{z_0}^{z_1} dz \int_{U(z)}^{\infty} p(E, T) T_r(z) dE \cong \frac{1}{L} \int_{z_0}^{z_1} dz \int_{U(z)}^{E_m} p(E, T) T_r(z) dE, \quad (9)$$

where z_0 is the initial height of H_2 and z_1 is the minimum height for H_2 to remain at molecular state (equals to the critical height, z_c), as shown in Fig. 7(a). The length $L = z_1 - z_0$ is the normalization factor, which is the decrease of height with reference to Cu(001). The integration of the kinetic energy function is considered only for the case when $E \geq U(z)$. The term $T_r(z)$ is the probability that a H_2 molecule passes through the transversal potential $U(x, y)$ (Fig. 7(b)) at temperature T and height z , which can be obtained by the transfer matrix (TM) method combined with calculations based on statistical mechanics. Quantum tunneling is possible only when the vibrational energy $E_n \geq E_c$, where E_c is the energy difference between the molecular and dissociated state at a height z (Fig. 7(b)). The mathematical expression for transmission probability is

$$T_r(z) = \sum_{n=n_c}^{\infty} p_n \times T_r(E_n - E_c, z), \quad (10)$$

where $p_n = \frac{e^{-\beta E_n}}{Q}$, $\beta = \frac{1}{k_B T}$, $E_n = (n + \frac{1}{2})\hbar\omega$, $Q = \sum_{n=0}^{\infty} e^{-\beta E_n} = \frac{e^{\beta\hbar\omega/2}}{e^{\beta\hbar\omega} - 1}$, E_n is the n th vibrational energy level of H_2 within the harmonic approximation (frequency ω), and the value of $\hbar\omega$ can be obtained directly from DFPT calculations. Using the above expressions, the probability p_n can be expressed as

$$p_n = e^{-n\beta\hbar\omega} (1 - e^{-\beta\hbar\omega}). \quad (11)$$

The term $T_r(E_n - E_c, z)$ is the probability of a H_2 molecule passing through the transversal barrier $U(x, y)$ with the incident energy of $E_n - E_c$ when the H_2 molecule is at the height z . Similarly, the transmission probability can be calculated using the TM method. The barrier height is E_b , as depicted in Fig. 7(b). For numerical evaluation, good convergence of the integral is obtained when $E_m \approx 5E_b$.

At a given height z , the energy of the system is set to the zero point of potential energy when the H-H bond is broken (Fig. 7(b)). The difference between the lowest potential energy point at this height and the potential energy zero is labeled as E_c . It should be emphasized that only the energy levels with $E_n \geq E_c$ can produce

effective quantum tunneling, and the corresponding vibrational energy level is labeled as the n_c th excited state. The subscript of the summation is therefore $n \geq n_c$. In the case of $E_n < E_c$, evanescent waves of incident particles are expected, which decay exponentially with the distance travelled. Finally, at temperature T , the total probability of H_2 dissociation on Cu(001) as a quantum particle is given by $P_Q(T) = P_{\perp}(T) + P_{\parallel}(T)$.

The role of quantum tunneling can be demonstrated by assuming the H_2 molecule to be a classical particle and compare the probability of dissociation at given temperatures. Similarly, dissociation can be considered as due to contributions from two processes. The first process is to overcome the potential barrier $U(z)$ to reach the decomposed adsorption state when H_2 gradually approaches the Cu(001) surface along the z direction. The probability corresponding to this process can be calculated as follows [43]:

$$P_{C\perp} = \int_{E_{b\perp}}^{\infty} p(E_k) dE_k = (1 - \text{Erf}[\sqrt{E_{b\perp}/(k_B T)}]) + \frac{2}{\sqrt{\pi}} \sqrt{E_{b\perp}/(k_B T)} e^{-\frac{E_{b\perp}}{k_B T}}. \quad (12)$$

As mentioned above, $p(E_k) = 2\pi \left(\frac{1}{\pi k_B T}\right)^{\frac{3}{2}} \sqrt{E_k} e^{-E_k/(k_B T)}$ is the kinetic energy distribution function at a given temperature T , E_k is the kinetic energy, and $E_{b\perp}$ corresponds to the height of $U(z)$, which is ~ 0.586 eV.

The second process is the dissociation due to the thermal motions of a single H atom, overcoming the constraint of H-H bond. The probability of this process is given by: $P_{C\parallel} = e^{-\frac{E_{b\parallel}}{k_B T}}$, where $E_{b\parallel} = E_{H-H}$ is the H-H bond energy (experimental data [62]: $E_{b\parallel} \sim 436$ kJ/mole or equivalently, $E_{b\parallel} \sim 4.51$ eV). This value is well above $E_{b\perp}$ and thus one has $P_{C\perp} \gg P_{C\parallel}$. Therefore, dissociation in the horizontal direction is negligible compared to that in the vertical (surface normal) direction due to the translational motions of H_2 . In summary, as a classical particle, the dissociation probability of H_2 is given by $P_c = P_{C\perp} + P_{C\parallel} \cong P_{C\perp}$. The calculated transmission probabilities are presented in Fig. 8, as a function of temperature. It is seen that both quantum and classical probabilities increase with elevating temperatures. Below $T = 1350$ K, the transmission probability taking into account quantum tunneling effects

(P_Q) is always higher than the case of treating the H_2 molecule as a classical particle (P_C). This phenomenon is even more pronounced at room temperature and below, at which the quantum transmission probability P_Q is well above its classical counterpart P_C . The lower panels of Fig. 8 compare the contribution of the two processes. It is found that the first process plays a major role in the overall dissociation, especially at low temperatures. At $T \leq 18$ K, the probability of the first process is more than 100 orders of magnitude higher than that of the second one.

Using the calculated dissociation probability of the H_2 molecule on Cu(001), we can estimate the rate constants of dissociation. The reaction rate constant k can be obtained via the following relation [43]: $k = \nu P$, where ν is the attempting frequency and P is the corresponding dissociation probability. For the first process, ν can be expressed as the reciprocal of the time $\tau(E)$ for travelling from the starting point z_0 to the end point z_1 (Fig. 7(a)). The dissociation rate constant for the first process is:

$$\nu_{\perp}(E) = \frac{1}{\tau(E)} = \frac{1}{\int_{z_0}^{z_1} \sqrt{\frac{m}{2(U(z)-E)}} dz}, \quad (13)$$

where E is the kinetic energy of the incident particle, $U(z)$ is the dissociation potential along the vertical direction as shown in Fig. 7(a), and m is the mass of H_2 molecule. The traversal time $\tau(E)$ of tunneling across the barrier is obtained using the formula presented in Ref. [63]. The reaction rate constant of the first process is

$$k_{\perp}(T) = \int_0^{\infty} \nu_{\perp}(E) p(E, T) T_r(E) dE \cong \int_0^{E_m} \nu_{\perp}(E) p(E, T) T_r(E) dE. \quad (14)$$

Like above, $E_m = 5E_b$ is adopted for numerical evaluation of the integral, and the kinetic energy distribution $p(E, T) = 2\pi \left(\frac{1}{\pi k_B T}\right)^{3/2} \sqrt{E} e^{-E/k_B T}$, for temperature T .

For the second process, the term ν is the frequency of the H-H stretching mode in the transverse direction, $\nu_{\parallel}(z)$, which varies with height z . In fact, $\nu_{\parallel}(z)$ gets progressively smaller with decreasing height z . The rate constant for the second process is given by

$$k_{\parallel}(T) = \frac{1}{L} \int_{z_0}^{z_1} dz \int_{U(z)}^{\infty} \nu_{\parallel}(z) p(E, T) T_r(z) dE \cong \frac{1}{L} \int_{z_0}^{z_1} dz \int_{U(z)}^{E_m} \nu_{\parallel}(z) p(E, T) T_r(z) dE, \quad (15)$$

where the vibrational frequency $\nu_{\parallel}(z)$ can be obtained from DFPT calculations. Ultimately, the total rate constant is

$$k_Q = k_{\perp}(T) + k_{\parallel}(T). \quad (16)$$

The results are shown in Fig. 9. It is seen from the reaction rate constant that dissociation in the vertical direction dominates the whole process. On the other hand, it is seen that (insets of Fig. 9) dissociation due to H-H vibrations (horizontal stretching) plays a nontrivial role at $T \geq 300$ K, for which both the translational and vibrational motions of H_2 contribute significantly to the breaking of H-H bond.

At a temperature $T_d = 220$ K (insets of Fig. 9), the rate constant of dissociation is $k_Q \sim 300/\text{s}$, which corresponds to a dissociation number of $N_{H_2} \approx 1.08 \times 10^6$ in one hour. The smallest face-centered two-dimensional (2D) surface unit cell of Cu(001) is a square with the side length of $a \sim 3.61$ Å and surface area $S_{\text{Cu}(001)} = a^2 \cong 13.03$ Å². Periodic extension by 1000 times along the two basis vectors gives a square substrate with a side length of $L \sim 0.361$ μm, which is comparable to size of samples employed experimentally. On average, each 2D surface unit cell can adsorb 1.08×2 H atoms. Define that adsorption of one H to one surface Cu gives a surface coverage of one monolayer (ML); then at $T_d = 220$ K, the surface coverage within one hour on Cu(001) is estimated to be ~ 1.13 ML. This is experimentally measurable, and nontrivial dissociation of H_2 is expected to take place on Cu(001) at $T \geq T_d$. The predicted temperature for the onset of nontrivial dissociation of H_2 , $T_d = 220$ K, is comparable with previous experimental observations of thermal desorption of dissociated H from Cu(001) ($T_d \sim 218$ K) [15]. Significant increase in the reaction rate constant is found when the temperature reaches 1000 K and above (Fig. 9), in which dissociation due to the stretching mode of H-H vibrations starts to play a nontrivial role. This is also in good agreement with the previous experimental measurements. When the kinetic energies of the hydrogen molecules ejected from the molecular beam nozzle reached about an equivalent temperature of ~ 1000 K and above, it was observed that hydrogen began to adsorb instantaneously on the copper surfaces with measurable sticking coefficients [6].

The kinetic processes studied above are based on the precondition that the dosed H_2 molecules are in thermal equilibrium with well-defined kinetic energy distribution

[43]. The situation changes significantly when the incident H_2 molecules are produced by molecular beam nozzle [6, 10], in which the kinetic energy of H_2 molecules distributes within a narrow range [10] and can be approximately taken as single-valued. For the monoenergetic molecular beams of H_2 with kinetic energy E , the probability of tunneling is given by the transmission coefficient $T_r(E)$, which is readily computed using the TM method. For a H_2 molecule which penetrates the barrier $U(z)$ and arrives at the $\text{Cu}(001)$, the rate constant of dissociation $k_{mbz}(E) = v_{\perp}(E) \times P_{\perp}(E) = v_{\perp}(E) \times T_r(E)$. We have made comparison on the rate constant of dissociation of H_2 under thermal equilibrium and the non-equilibrium molecular beam experiment. The characteristic temperature for the activation of rotation degree of freedom of a H_2 molecule is $\theta_r \sim 85$ K [64]. By contrast, the vibrational degree of freedom of H_2 is largely frozen at its ground state due to the very high characteristic temperature ($\theta_v \sim 6100$ K) [64]. For temperatures above θ_r , both the translational and rotational degree of freedom of H_2 are activated, and the equivalent temperature of the incident H_2 molecular beam with kinetic energy E can therefore be estimated to $T = \frac{2E}{5k_B}$. The calculated rate constants are shown in Fig. 10, as a function of temperature and the kinetic energy of each H_2 from molecular beams. It is clearly seen that at the same temperature the rate constant under thermal equilibrium (k_Q) is larger than that of molecular beams (k_{mbz}). Compared to monoenergetic molecular beam with the translational kinetic energy E_t , the H_2 molecules at thermal equilibrium have a nontrivial probability of being at the energy states $E \geq E_t$, which is $P(E \geq E_t) = \int_{E_t}^{\infty} p(E) dE \cong \frac{2}{\sqrt{\pi}} \sqrt{E_t/(k_B T)} e^{-(\frac{E_t}{k_B T})}$. Recalling that $E_t = \frac{3k_B T}{2}$, we have $P(E \geq E_t) \cong \frac{2}{\sqrt{\pi}} \sqrt{3/2} e^{-(\frac{3}{2})} \cong 0.308$. This means that a considerable portion of H_2 molecules possess kinetic energies above the average E_t , and explains the difference between k_Q and k_{mbz} . Using the experimental parameters presented in Ref. [10], i.e., the flux of the incident H_2 molecular beam through the nozzle (with diameter $d = 3$ mm) is $\sim 10^{15}/\text{sec}$, the number of incident H_2 molecules per second for unit area is estimated to be $F_{mbz} = \frac{N_{\text{H}_2}}{S_{mbz}} = \frac{N_{\text{H}_2}}{\pi(\frac{d}{2})^2} = \frac{10^{15}}{\pi \times 2.25 \times 10^{14}} \cong 1.41/\text{\AA}^2$. Within a time t , the number of H_2

molecules deposited on the surface unit cell of Cu(001) is therefore

$$n_{d,H_2}(E) = F_{mbz} \times S_{Cu(001)} \times k_{mbz}(E) \times t \quad (17)$$

In the case $t = 1$ sec, $n_{d,H_2}(E) \cong 18.4 \times k_{mbz}(E)$. Our calculations give that, for the kinetic energy $E = 0.176$ eV, $k_{mbz}(E) \cong 0.073/\text{sec}$, and $n_{d,H_2}(0.176) \cong 1.3$, which implies that the surface coverage of dissociatively adsorbed H is ~ 1 ML. This is expected to give detectable signals for experimental measurements. The threshold value of $E = 0.176$ eV for measurable dissociative adsorption of H_2 on Cu(001) is comparable with the experimental data ($E = 0.2$ eV) based on molecular beam measurements [6]. The result points to the key role of quantum tunneling in the activated dissociation of H_2 on Cu(001).

3.3. The Effective barrier and isotope effects

For the barrier-crossing process of a microscopic particle that satisfies the Van't Hoff-Arrhenius relation, the total transmission probability (P_{tot}) can be generally expressed as follows [43]:

$$P_{tot}(T) = e^{-E_b^*/(k_B T)}, \quad (18)$$

where E_b^* is the effective barrier, and k_B , T have the usual meanings as before. Therefore, the value of the effective barrier E_b^* can be obtained as follows:

$$E_b^* = -(k_B T) \ln[P_{tot}(T)] = k_B T \ln\left[\frac{1}{P_{tot}(T)}\right]. \quad (19)$$

Clearly, the effective barrier E_b^* is a function of temperature. Using the probability $P_{tot}(T)$ obtained by the TM method, the values of E_b^* at different temperatures are calculated and shown in Fig. 11. The data for the dissociation of H_2 and D_2 are presented, to show the isotope effects. It is seen that the effective barrier E_b^* which taking into account the effects of quantum tunneling is appreciably lower than the classical barrier height (dissociation along the surface normal, $U(z)$) which is deduced by treating the motions of incident H_2 molecules as classical particles. For $T \geq 200$ K, the effective dissociation barriers of both H_2 and D_2 increase smoothly with T and arrive at their maxima at ~ 500 K, then decrease slowly with further increasing

temperatures. The nearly steady gap ($\Delta E = E_{b_{H_2}}^* - E_{b_{D_2}}^* \sim 0.02$ eV) between the effective barriers of H_2 and D_2 is a consequence of quantum tunneling, whose probability decreases with increasing particle mass. The existence of a maximum of E_b^* can be qualitatively understood based on Eq. (19), where the competition between the term $k_B T$ and $\ln[\frac{1}{P_{tot}(T)}]$ arrives at a compromise [43]. The weak temperature dependence of E_b^* at $T \geq 300$ K indicates that it is usually sufficient to use one barrier parameter to describe the temperature-dependent kinetic process of atoms.

From $T \sim 200$ K to 260 K, the effective barrier for H_2 (D_2) increases slightly from $E_b^* \sim 0.47$ (0.49) eV to $E_b^* \sim 0.48$ (0.50) eV. This is comparable with the data from thermal desorption (reverse process of dissociation) measurements in the same range of temperature, in which the activation barrier of dissociation is determined to be 48 ± 6 kJ/mol ($\sim 0.50 \pm 0.06$ eV) for H_2 and 56 ± 8 kJ/mol (0.58 ± 0.08 eV) for D_2 , respectively. The situation is much different for $T \leq 200$ K. The effective barrier drops almost linearly with decreasing temperature. From 200 K to 10 K, the effective barrier for H_2 (D_2) decreases quickly from $E_b^* \sim 0.47$ (0.49) eV to $E_b^* \sim 0.06$ (0.08) eV. When the temperature T approaches 0 K, E_b^* tends to be zero, which reveals that quantum tunneling effects may have a significant impact on the atomic scale dynamics even at extremely low temperatures.

The significant role of quantum tunneling can be further demonstrated by investigating the isotope effects on the transmission probability and rate constant of H_2 and D_2 dissociation on Cu(001). In calculations based on the TM method, both H_2 and D_2 are treated as quantum particles, for a temperature range of $T \leq 300$ K. The results are shown in Fig. 12. In the low temperature region, in particular, $T \leq 100$ K, significant differences between the transmission probabilities and rate constants are found. Using the relation $k = \nu P_Q$, the natural logarithm of reaction constant, $\ln(K_Q)$ may be expressed as follows

$$\ln(K_Q) = \ln(\nu P_Q) = \ln\left(\nu e^{-\frac{E_b^*}{k_B T}}\right) = \ln \nu - \frac{E_b^*}{k_B T}, \quad (20)$$

where the minus slope of the $\ln(K_Q) \sim \frac{1}{k_B T}$ lines simply corresponds to the

effective barrier E_b^* at a given temperature T . As seen from Fig. 12(d), the turning point at $T \sim 100$ K distinguishes the rate constants of H_2 from D_2 , an indication of crossover from classical to quantum regime. Moreover, the variation trends of the two curves can be roughly described by the combination of two lines with the slopes being equivalent to two effective barriers, as schematically shown by the dash lines in Fig. 12(d). Similar characteristics of T -dependent rate constant are found in the case of H diffusion on Cu(001) and Pt(111) surfaces [65-67], and may be expected for diffusion processes on the other metal surfaces. In phenomenological descriptions of the effects of quantum tunneling [68, 69], two sets of parameters for the activation barriers (one for classical and one for quantum motions) plus two prefactors are introduced which roughly account for the dynamics at high and low temperature regions. By contrast, our method produces the major features of the variations of rate constant with temperature in a logically natural and unified manner, and provides a promising way for including the effects of quantum tunneling in the chemical dynamics of many-body systems.

The transmission coefficients $T_r(E)$, the total transmission probability $P_{tot}(T)$ at given temperature T , the rate constants k , and the corresponding effective barrier E_b^* are deduced based on the PES calculated at the DFT-GGA level. When a more accurate PES for the H_2 -Cu(001) interactions (e.g. the PES calculated by the semi-empirical SRP-DFT approach [32-35]) is employed, or when the van der Waals corrections are introduced, or when the interactions due to surface phonons are included [34]: All of which may be taken as perturbations to the PES obtained by DFT-GGA calculations. As has been shown [43] that perturbations/small changes to the original PES would only result in minor modifications on the transmission coefficients $T_r(E)$, and therefore the quantities derived based on $T_r(E)$. Consequently, the main results regarding the role of quantum tunneling in the dissociation kinetics of H_2 on Cu(001) are qualitatively kept unchanged.

4. Concluding Remarks

In summary, the activation and dissociation processes of H_2 molecules on

Cu(001) surface have been studied based on first-principles calculations and the transfer matrix (TM) method. It is found that charge transfer from the substrate Cu atoms to H_2 plays an essential role in activating and breaking the H-H bond. The competition between the H-H and H-Cu interactions at electronic level is quantified by comparing the 1s-1s of H-H and 1s-4s of H-Cu orbital overlap integrals at the critical position of dissociation. Using the PES determined by DFT calculations, the probabilities of H_2 molecules passing through the dissociation energy pathways are calculated using the TM method, which explicitly taking into account the effects of quantum tunneling. The probabilities and rate constants of dissociation due to the translational and vibrational motions are evaluated and distinguished. Both translational and vibrational motions contribute nontrivially to the dissociation of H_2 at high temperatures. For the situation where the Van't Hoff-Arrhenius relationship applies, the effective potential for the dissociation and adsorption of H_2 on Cu(001) is calculated. After considering the effects of quantum tunneling, the barrier height is significantly reduced with comparison to that of the barrier which treats the H_2 as a classical particle within the Born-Oppenheimer approximation. In studies for the situation of thermal equilibrium and the non-equilibrium molecular beam of H_2 , the calculated temperatures for the onset of measurable dissociation of H_2 on Cu(001) are in agreement with experiments. To further demonstrate the role of quantum tunneling, we have computed the effective barriers of dissociation for both H_2 and D_2 which are found to be comparable with experimental data. The role of quantum effects is found to be remarkable at low-temperature region in which the crossover from classical to quantum regime is identified. The results are expected to be tested by future experimental works.

Acknowledgements

This work is financially supported by the National Natural Science Foundation of China (No. 11474285, 12074382). We are grateful to the staff of the Hefei Branch of Supercomputing Center of Chinese Academy of Sciences, and the Hefei Advanced Computing Center for support of supercomputing facilities.

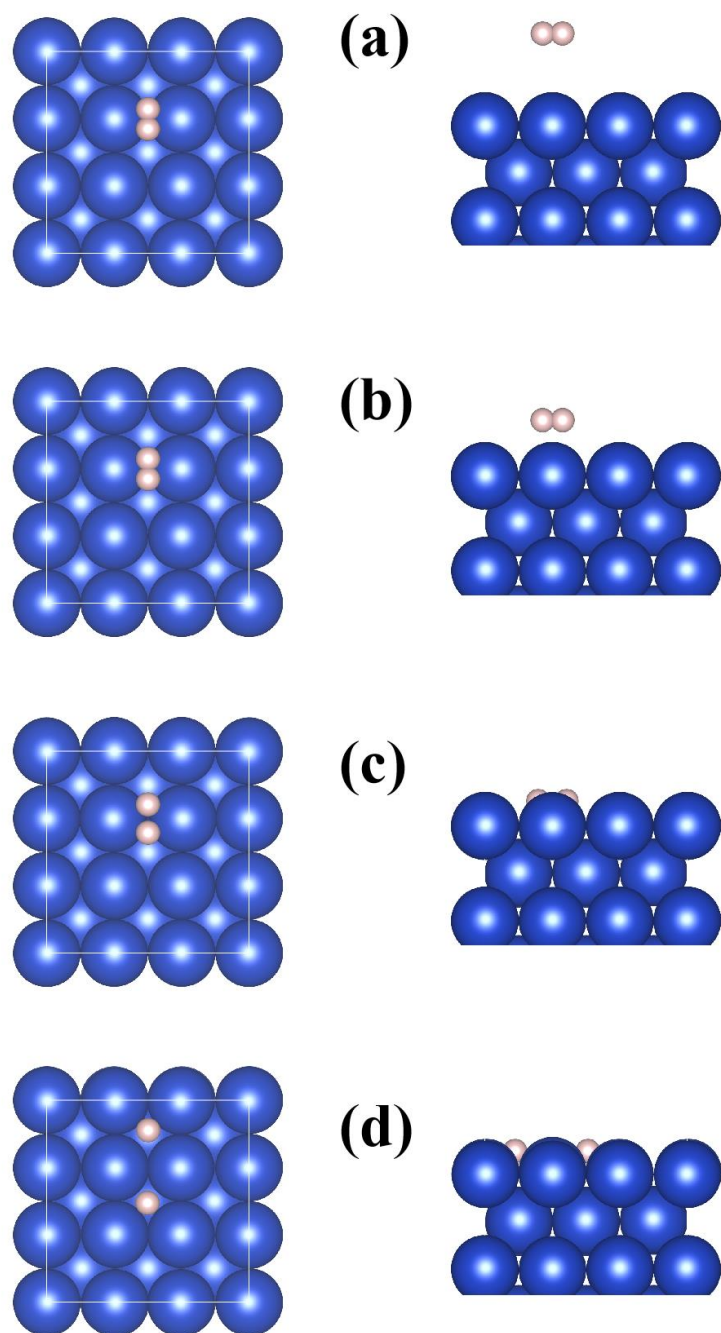


Figure 1. Top (left) and side views (right) of typical H_2/Cu (001) configurations from the molecular state to the dissociation state. The blue (large) balls represent for Cu atoms while the pink (small) one for H atoms. This convention applies to all the figures.

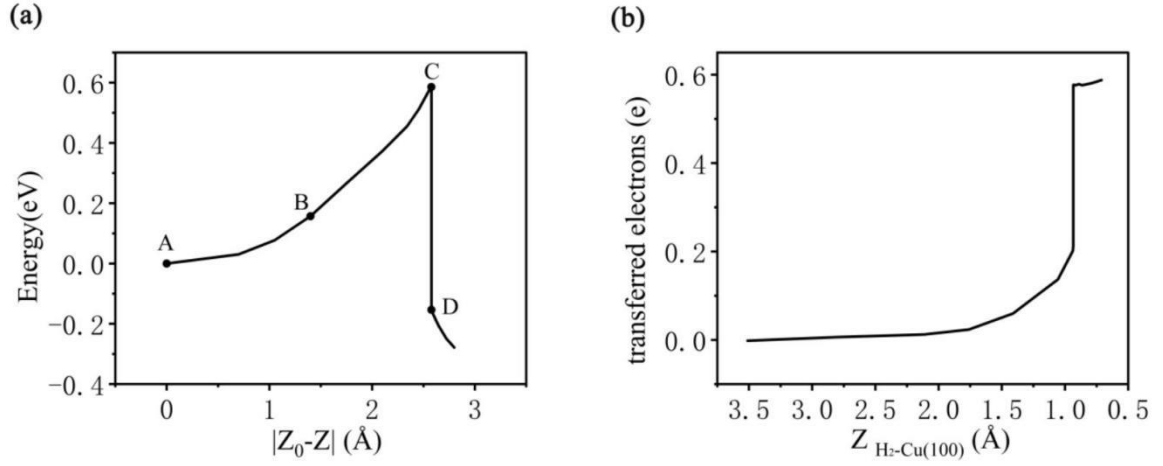


Figure 2. (a) Calculated potential energy $U(z)$ when a H_2 molecule gradually approaches $\text{Cu}(001)$ surface. The letters A-D correspond respectively to the configurations shown in Figs. 1(a)-(d). Z_0 is the initial height of the H_2 molecule and $|Z_0 - Z|$ is the distance travelled from the initial position. (b) Charge transfer from $\text{Cu}(001)$ to H_2 based on Bader analysis, as a function of $Z_{\text{H}_2-\text{Cu}(100)}$, the distance from H_2 to the $\text{Cu}(001)$.

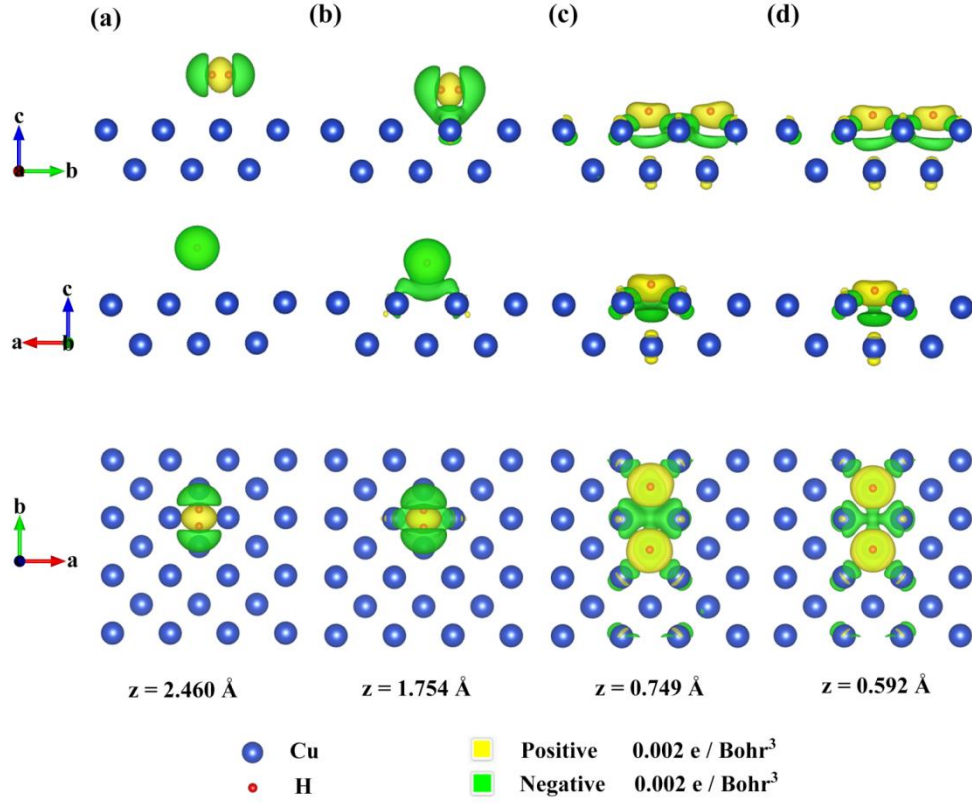


Figure 3. Isosurfaces of charge density difference for the $\text{H}_2/\text{Cu}(001)$ at gradually decreasing $\text{H}_2\text{-Cu}(001)$ distances. **(a)** The initial configuration of H_2 , corresponding to the configuration in Fig. 1(a) and point A in Fig. 2(a). **(b)** The transition state of H_2 from molecular state to dissociation state. **Panels (c) and (d):** The dissociation states in the form of adsorbed H atoms on $\text{Cu}(001)$, with panel (d) being the final stable dissociation state.

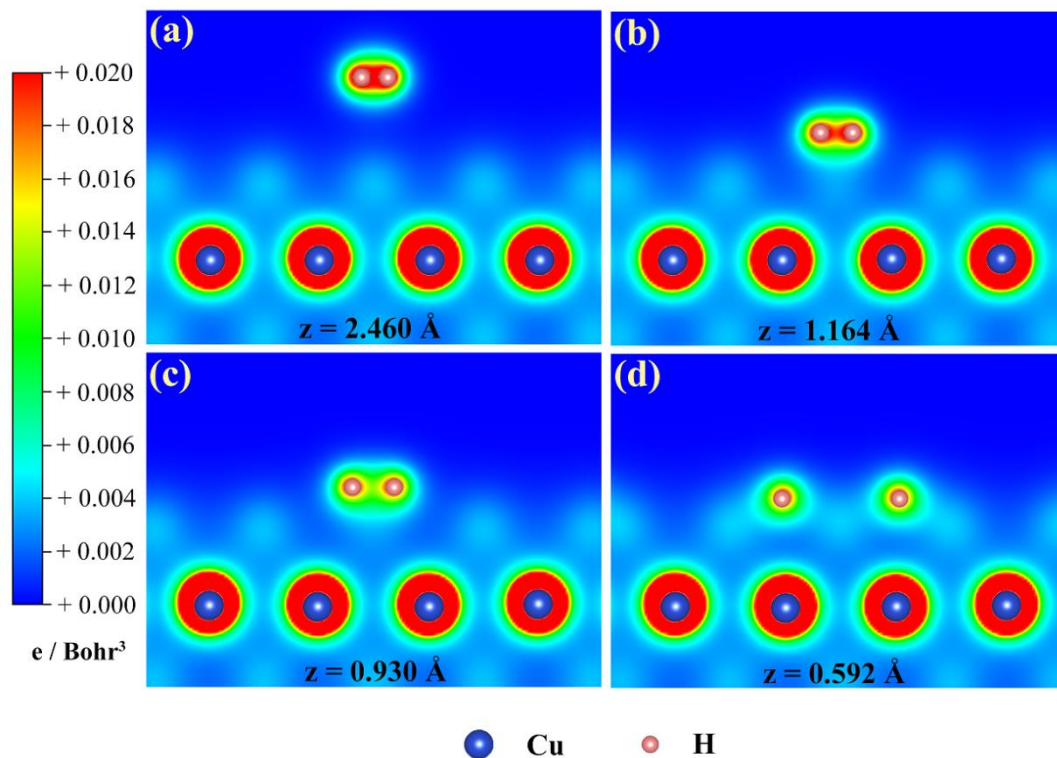


Figure 4. Two-dimensional (2D) contours of charge densities associated with the breaking of H-H bond. (a) The molecular state of H_2 . (b) & (c) The transition states of H_2 . (d) Dissociative state of H_2 on the $\text{Cu}(001)$ surface.

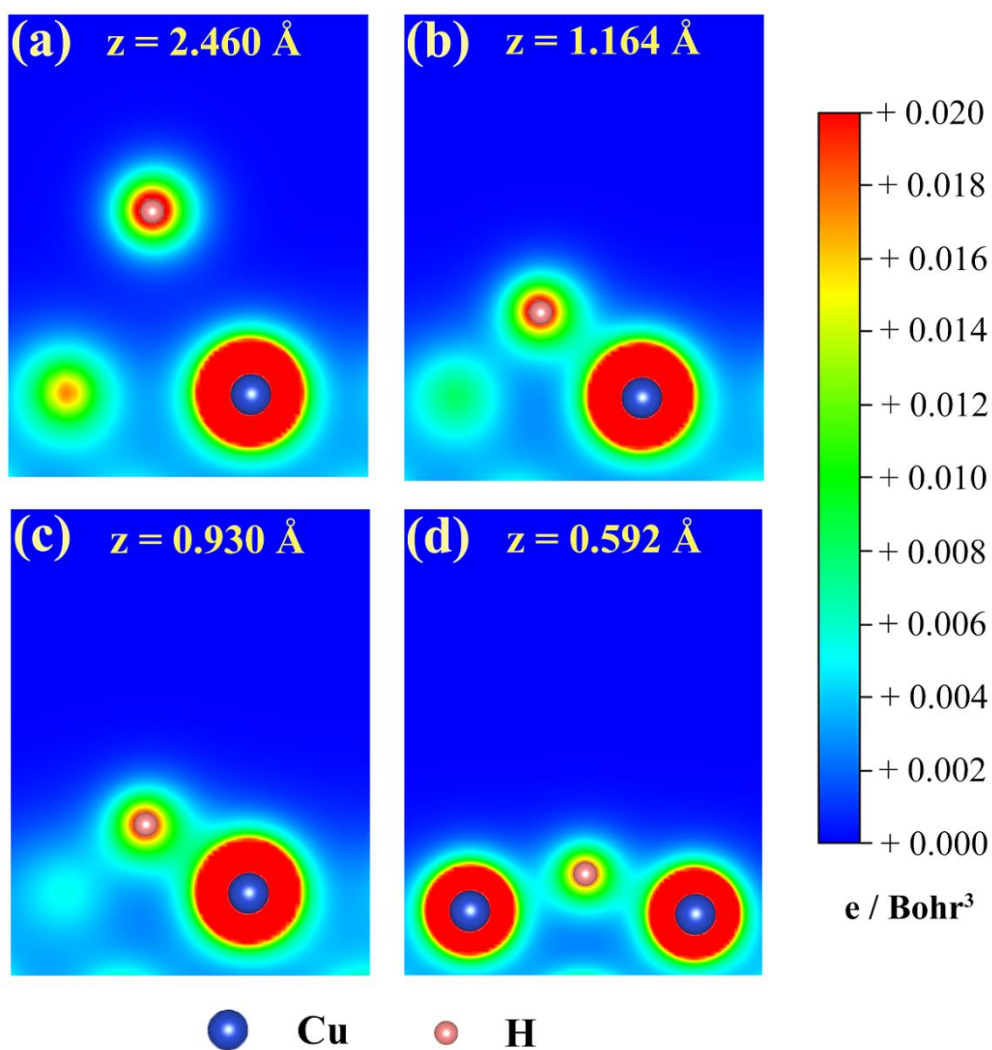


Figure 5. Two-dimensional (2D) contours of charge densities illustrating the formation of H-Cu bond, for the same configurations as shown in Fig. 4 but viewed from different perspective angles.

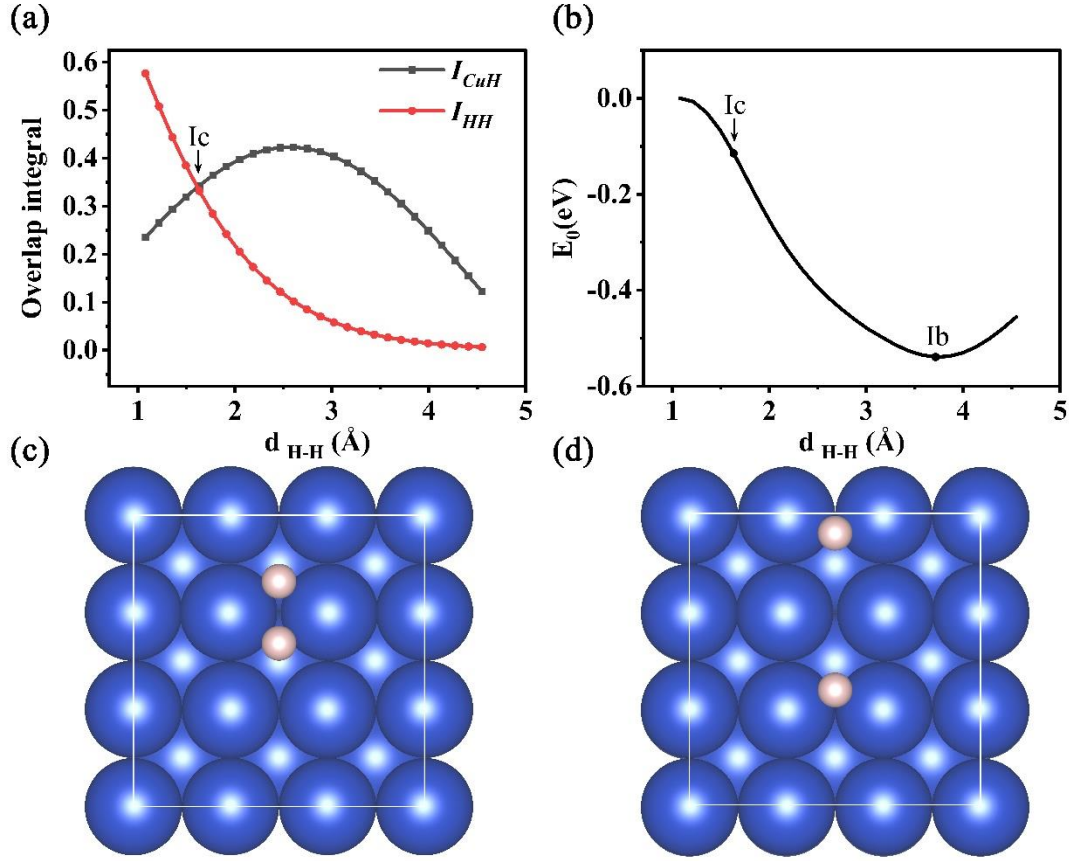


Figure 6. (a) Calculated integrals describing the overlap of 1s-1s orbitals of H-H and the 1s-4s orbitals of H-Cu, as a function of the H-H separations at the corresponding atomic configurations when the H_2 molecule approaches the Cu(001). (b) Variation of relative energies of the $\text{H}_2/\text{Cu}(001)$ system at approximately the critical height of bond breaking, as a function of the H-H separations. Ic corresponds to the case where both H-H bonds and H-Cu bonds present. Lower panels (c) and (d) display the top views of Ic and Ib marked in upper panels (a) and (b), respectively.

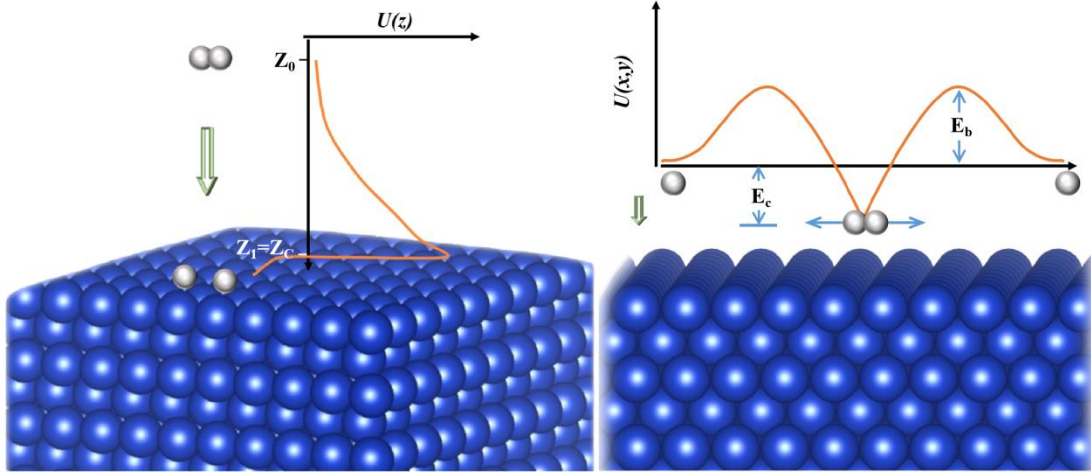


Figure 7. Schematic diagrams for **(a)** Dissociation of H₂ molecules incident along the surface normal (z) directions. Z_C and Z_0 correspond to the initial position of H₂ and the critical position (point C in Fig. 2(a)). **(b)** The dissociation of H₂ molecules along the transverse direction. The potential energy difference between the instantaneous ground-state energy of H₂ at height z and the potential energy zero point (completely dissociative state) is marked as E_c . The potential barrier height to be overcome with reference to potential energy zero is marked as E_b .

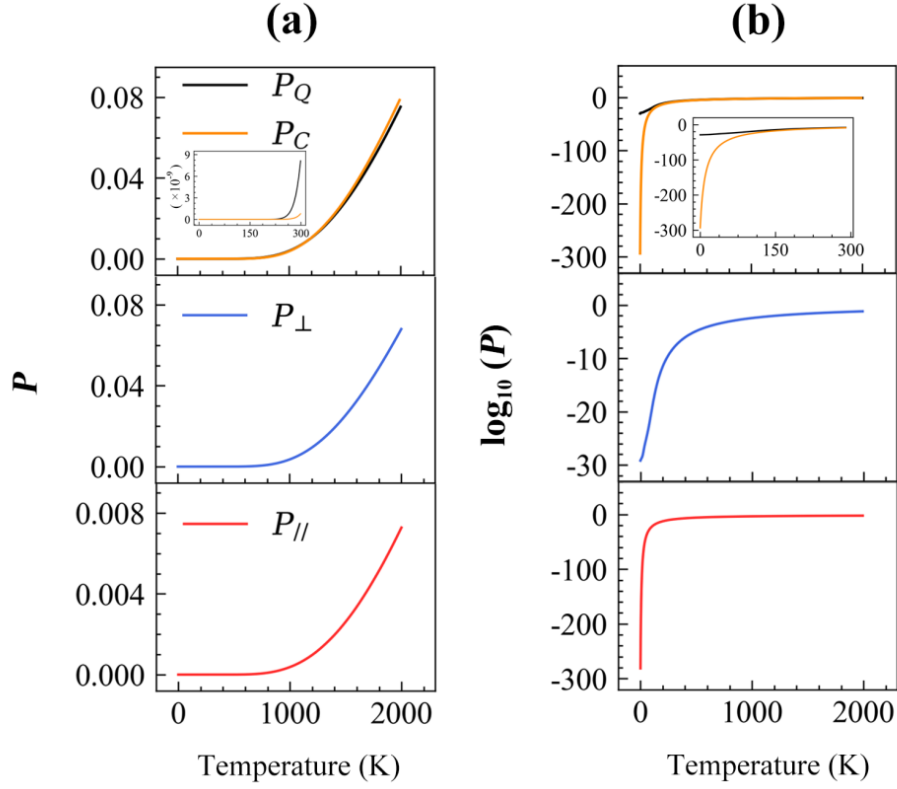


Figure 8. The probability (panel (a)) and logarithms (panel (b)) of H₂ dissociation due to the translational motions in surface normal (vertical) direction (subscript \perp) and vibrations in the transverse direction (subscript \parallel) on Cu(001). The classical (P_C) and quantum probability (P_Q) are compared as a function of temperature.

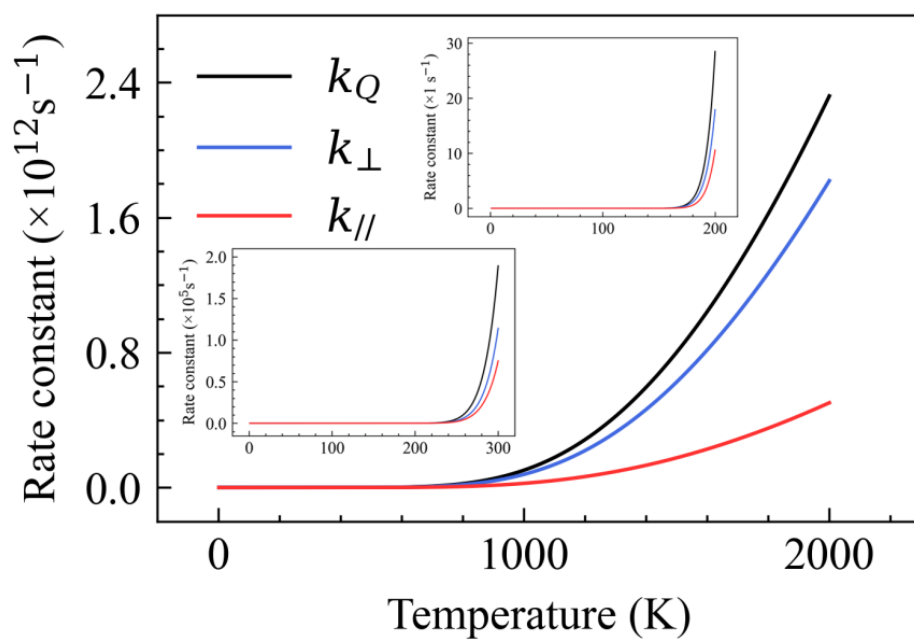


Figure 9. Temperature dependence of quantum rate constant k_Q , and their vertical and transverse components.

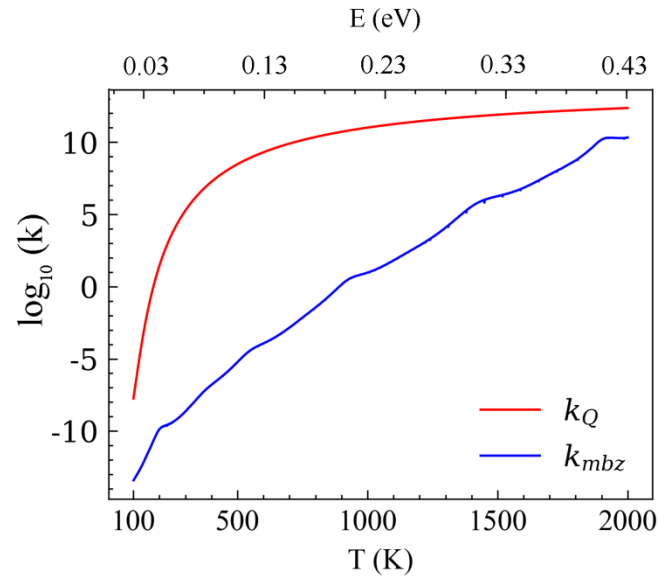


Figure 10. Calculated rate constants k (in logarithms) for the dissociation of H_2 on Cu(001), under the situation of thermal equilibrium (k_Q) and molecular beam experiments (k_{mbz}).

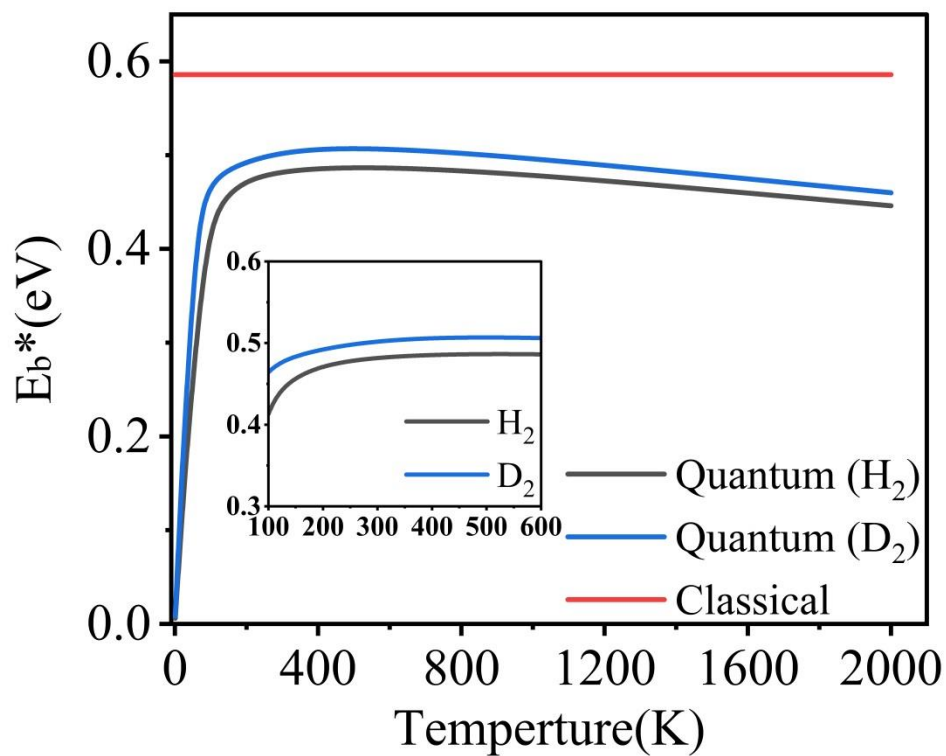


Figure 11. The energy barriers for the dissociation of H₂ and D₂ on Cu(001). The original barrier height calculated using adiabatic approximation is referred to as “Classical”. The effective barriers (E_b^*) due to quantum effects are presented as a function of temperature.

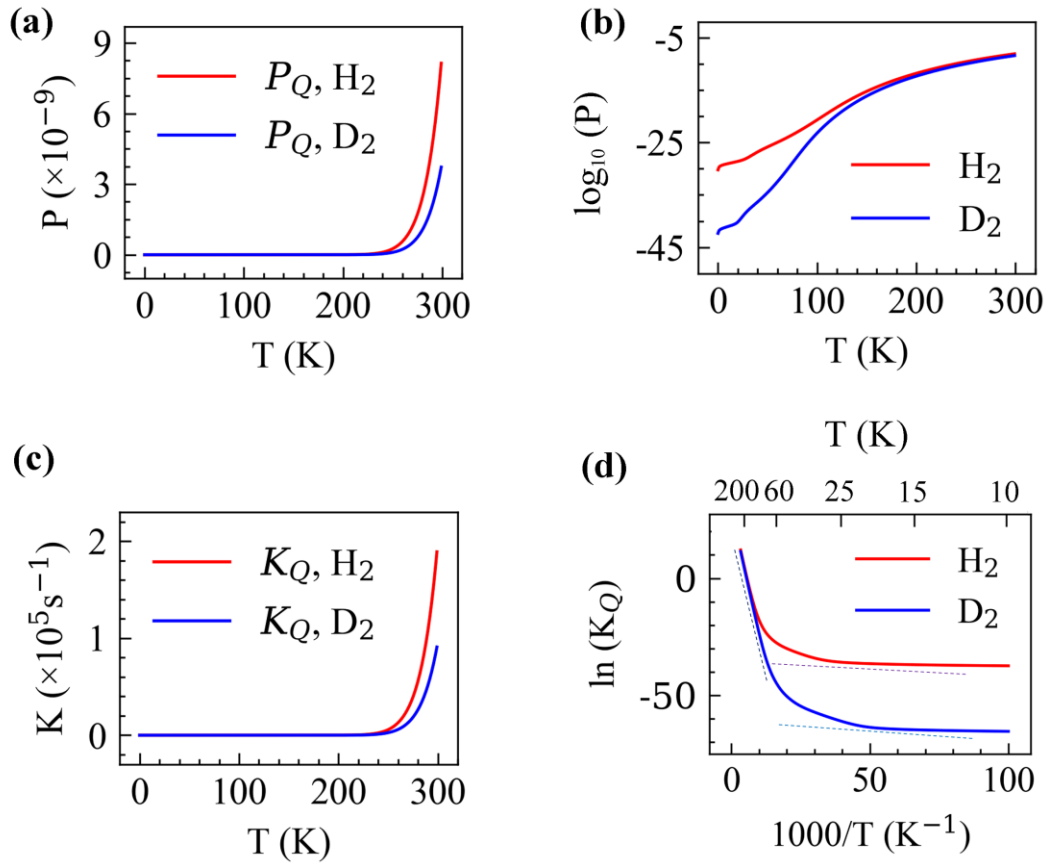


Figure 12. Calculated quantum probabilities (upper panels) and rate constants (lower panels) for H₂ and D₂ dissociation on Cu(001), as function of temperature. The crossover from classical to quantum regime is schematically indicated by dash lines (panel (d)).

References:

- [1] I. Swart, F. M. F. de Groot, B. M. Weckhuysen, P. Gruene, G. Meijer, A. Fielicke, H₂ Adsorption on 3d Transition Metal Clusters: A Combined Infrared Spectroscopy and Density Functional Study, *J. Phys. Chem. A* **112**, 1139 (2008).
- [2] J. Zhao, P. Qi, X. Jie, F. Tao, Current Situation and Prospect of Hydrogen Storage Technology with New Organic Liquid, *Int. J. Hydrog. Energy* **39**, 17442 (2014).
- [3] M. S. Hou, S. Q. Li, R. Zhu, R. Z. Liu, Y. G. Wang, Experiment Research of Non-Carbon Metallurgy with Clean Energy, *Adv. Mat. Res.* **803**, 355 (2013).
- [4] M. Salmeron, R. J. Gale, G. A. Somorjai, Molecular Beam Study of the H₂–D₂ Exchange Reaction on Stepped Platinum Crystal Surfaces: Dependence on Reactant, *J. Chem. Phys.* **67**, 5324 (1977).
- [5] H. C. Kang, W. H. Weinberg, Modeling the Kinetics of Heterogeneous Catalysis, *Chem. Rev* **95**, 667 (1995).
- [6] G. Anger, A. Winkler, K. D. Rendulic, Adsorption and Desorption Kinetics in the Systems H₂/Cu(111), H₂/Cu(110), H₂/Cu(100), *Surf. Sci.* **220**, 1 (1989).
- [7] K. Besocke, B. Krah-Urban, H. Wagner, Dipole Moments Associated with Edge Atoms; A Comparative Study on Stepped Pt, Au and W Surfaces, *Surf. Sci.* **68**, 39 (1977).
- [8] R. J. Behm, K. Christmann, G. Ertl, Adsorption of Hydrogen on Pd (100), *Surf. Sci.* **99**, 320 (1980).
- [9] J. P. Jardin, M. C. Desjonquères, D. Spanjaard, Adsorption of Simple Elements on a Stepped bcc Transition Metal Surface, *Surf. Sci.* **162**, 224 (1985).
- [10] M. Balooch, M. J. Cardillo, D. R. Miller, R.E. Stickney, Molecular Beam Study of the Apparent Activation Barrier Associated with Adsorption and Desorption of Hydrogen on Copper, *Surf. Sci.* **46**, 358 (1974).
- [11] J. Tersoff, L. M. Falicov, Electronic Structure and Local Atomic Configurations of Flat and Stepped (111) Surfaces of Ni and Cu, *Phys. Rev. B* **24**, 754 (1981).
- [12] X. Shen, Y. Li, X. Liu, D. Zhang, J. Gao, T. Liang, Hydrogen Diffusion into the Subsurfaces of Model Metal Catalysts from First Principles, *Phys. Chem. Chem. Phys.* **19**, 3557 (2017).

- [13] P. Ferrin, S. Kandoi, A. U. Nilekar, M. Mavrikakis, Hydrogen Adsorption, Absorption and Diffusion on and in Transition Metal Surfaces: a DFT study, *Surf. Sci.* **606**, 679 (2012).
- [14] C. S. Alexander, J. Pritchard, Chemisorption of Hydrogen on Evaporated Copper Films, *J. Chem. Soc., Faraday Trans. 1*, **68**, 202 (1972).
- [15] P. B. Rasmussen, P. M. Holmblad, H. Christoffersen, P.A. Taylor, I. Chorkendorff, Dissociative Adsorption of Hydrogen on Cu(100) at Low Temperatures, *Surf. Sci.* **287/288**, 79 (1993).
- [16] Q. Sun, J. J. Xie, T. Zhang, Chemisorption of Hydrogen on Stepped (410) Surfaces of Ni and Cu, *Surf. Sci.* **338**, 11 (1995).
- [17] J. J. Xie, P. Jiang, K. M. Zhang, The Dissociative Adsorption of H₂ on Cu (100): Orientation Dependence and Impurity Effects, *J. Phys.: Condens. Matter* **6**, 7217 (1994).
- [18] J. J. Xie, P. Jiang, K. M. Zhang, Dynamics of H₂ Dissociation on Cu (100): Effects of Surface Defects, *J. Chem. Phys.* **104**, 9994 (1996).
- [19] M. F. Somers, D. A. McCormack, G. J. Kroes, R. A. Olsen, E. J. Baerends, R. C. Mowrey, Signatures of Site-specific Reaction of H₂ on Cu (100), *J. Chem. Phys.* **117**, 6673 (2002).
- [20] K. Christmann, G. Ertl, T. Pignet, Adsorption of Hydrogen on a Pt(111) Surface, *Surf. Sci.* **54**, 365 (1976).
- [21] D. Hennig, S. Wilke, R. Löber, M. Methfessel, The Adsorption of Hydrogen on Pd (100) and Rh (100) Surfaces: a Comparative Theoretical Study, *Surf. Sci.* **287**, 89 (1993).
- [22] S. H. Payne, H. J. Kreuzer, W. Frie, L. Hammer, K. Heinz, Adsorption and Desorption of Hydrogen on Rh(311) and Comparison with Other Rh Surfaces, *Surf. Sci.* **421**, 279 (1999).
- [23] E. W. F. Smeets, J. Voss, G. J. Kroes, Specific Reaction Parameter Density Functional Based on the Meta-Generalized Gradient Approximation: Application to H₂ + Cu (111) and H₂ + Ag (111), *J. Phys. Chem. A* **123**, 5395 (2019).
- [24] J. Harris, S. Andersson, H₂ Dissociation at Metal Surfaces, *Phys. Rev. Lett.* **55**,

1583 (1985).

[25] J. Harris, On the Adsorption and Desorption of H_2 at Metal Surfaces. *Appl. Phys. A* **47**, 63 (1988).

[26] G. Wiesenekker, G. J. Kroes, E. J. Baerends, An Analytical Six-dimensional Potential Energy Surface for Dissociation of Molecular Hydrogen on Cu(100), *J. Chem. Phys.* **104**, 7344 (1996).

[27] G. J. Kroes, E. J. Baerends, R. C. Mowrey, Six-Dimensional Quantum Dynamics of Dissociative Chemisorption of ($y = 0, j = 0$) H_2 on Cu(100), *Phys. Rev. Lett.* **78**, 5383 (1997).

[28] G. J. Kroes, E. J. Baerends, R. C. Mowrey, Six-dimensional Quantum Dynamics of Dissociative Chemisorption of on Cu(100), *J. Chem. Phys.* **107**, 3309 (1997).

[29] D. A. McCormack, G. J. Kroes, R. A. Olsen, E. J. Baerends, R. C. Mowrey, Rotational Effects in Six-dimensional Quantum Dynamics for Reaction of on Cu(100), *J. Chem. Phys.* **110**, 7008 (1999).

[30] D. A. McCormack, G. J. Kroes, R. A. Olsen, E. J. Baerends, R. C. Mowrey, Rotational Effects on Vibrational Excitation of H_2 on Cu(100), *Phys. Rev. Lett.* **82**, 1410 (1999).

[31] R. A. Olsen, H. F. Busnengo, A. Salin, M. F. Somers, G. J. Kroes, E. J. Baerends, Constructing Accurate Potential Energy Surfaces for a Diatomic Molecule Interacting with a Solid Surface: $H_2 + Pt(111)$ and $H_2 + Cu(100)$, *J. Chem. Phys.* **116**, 3841 (2002).

[32] C. D áz, E. Pijper, R. A. Olsen, H. F. Busnengo, D. J. Auerbach, G. J. Kroes, Chemically Accurate Simulation of a Prototypical Surface Reaction: H_2 Dissociation on Cu(111), *Science* **326**, 832 (2009).

[33] L. Sementa, M. Wijzenbroek, B. J. van Kolck, M. F. Somers, A. Al-Halabi, H. F. Busnengo, R. A. Olsen, G. J. Kroes, M. Rutkowski, C. Thewes, N. F. Kleimeier, H. Zacharias, Reactive Scattering of H_2 from Cu(100): Comparison of Dynamics Calculations Based on the Specific Reaction Parameter Approach to Density Functional Theory with Experiment, *J. Chem. Phys.* **138**, 044708 (2013).

[34] A. Marashdeh, S. Casolo, L. Sementa, H. Zacharias, G. J. Kroes, Surface

- Temperature Effects on Dissociative Chemisorption of H₂ on Cu(100), *J. Phys. Chem. C* **117**, 8851 (2013).
- [35] G. J. Kroes, Toward a Database of Chemically Accurate Barrier Heights for Reactions of Molecules with Metal Surfaces, *J. Phys. Chem. Lett.* **6**, 4106 (2015).
- [36] S. M. Sharada, T. Bligaard, A. C. Luntz, G. J. Kroes, J. K. Nørskov, SBH10: A Benchmark Database of Barrier Heights on Transition Metal Surfaces, *J. Phys. Chem. C* **121**, 19807 (2017).
- [37] G. J. Kroes, Computational approaches to dissociative chemisorption on metals: towards chemical accuracy, *Phys. Chem. Chem. Phys.* **23**, 8962 (2021).
- [38] L. J. Zhu, Y. L. Zhang, L. Zhang, X. Y. Zhou, B. Jiang, Unified and transferable description of dynamics of H₂ dissociative adsorption on multiple copper surfaces via machine learning, *Phys. Chem. Chem. Phys.* **22**, 13958 (2020).
- [39] S. S. Lv, X. J. Liu, X. J. Shen, A simulated-TPD Study of H₂ Desorption on Metal Surfaces, *Surf. Sci.* **718**, 122015 (2022).
- [40] T. E. Markland and M. Ceriotti, Nuclear quantum effects enter the mainstream. *Nat. Rev. Chem.* **2**, 0109 (2018).
- [41] M. Ceriotti, W. Fang, P. G. Kusalik, R. H. McKenzie, A. Michaelides, M. A. Morales and T. E. Markland, Nuclear Quantum Effects in Water and Aqueous Systems: Experiment, Theory, and Current Challenges. *Chem. Rev.* **116**, 7529 (2016).
- [42] Y. Yang, Y. Kawazoe, Adsorption and Diffusion of H Atoms on β -PtO₂ Surface: The Role of Nuclear Quantum Effects, *J. Phys. Chem. C* **123**, 13804 (2019).
- [43] C. Bi, Y. Yang, Atomic Resonant Tunneling in the Surface Diffusion of H Atoms on Pt (111), *J. Phys. Chem. C* **125**, 464 (2021).
- [44] P. R. Schreiner, Quantum Mechanical Tunneling Is Essential to Understanding Chemical Reactivity, *Trends Chem.* **2**, 980 (2020).
- [45] J. Meisner, J. Kästner, Atom Tunneling in Chemistry, *Angew. Chem. Int. Ed.* **55**, 5400 (2016).
- [46] G. Kresse, J. Furthmüller, Efficient Iterative Schemes for ab initio Total-energy Calculations Using a Plane-wave Basis Set, *Phys. Rev. B* **54**, 169 (1996).
- [47] G. Kresse, J. Hafner, Ab initio Molecular Dynamics for Liquid Metals, *Phys. Rev.*

B **47**, 558 (1993).

[48] J. P. Perdew, Density-functional Approximation for the Correlation Energy of the Inhomogeneous Electron Gas, *Phys. Rev. B* **34**, 7406 (1986).

[49] J. P. Perdew, K. Burke, M. Ernzerhof, Generalized Gradient Approximation Made Simple, *Phys. Rev. Lett.* **77**, 3865 (1996).

[50] P. E. Blöchl, Projector Augmented-wave Method, *Phys. Rev. B* **50**, 17953 (1994).

[51] G. Kresse, D. Joubert, From Ultrasoft Pseudopotentials to the Projector Augmented-wave Method, *Phys. Rev. B* **59**, 1758 (1999).

[52] K. Momma, F. Izumi, VESTA 3 for Three-dimensional Visualization of Crystal, Volumetric and Morphology Data, *J. Appl. Crystallogr.* **44**, 1272 (2011).

[53] H. J. Monkhorst, J. D. Pack, Special Points for Brillouin-zone Integrations, *Phys. Rev. B* **13**, 5188 (1976).

[54] S. Baroni, R. Resta, Ab initio Calculation of the Macroscopic Dielectric Constant in Silicon, *Phys. Rev. B* **33**, 7017 (1986).

[55] L. I. Schiff, Quantum Mechanics (McGraw-Hill, New York, 1968), p. 268.

[56] B. W. J. Chen, M. Mavrikakis, How Coverage Influences Thermodynamic and Kinetic Isotope Effects for H₂/D₂ Dissociative Adsorption on Transition Metals. *Catal. Sci. Technol.* **10**, 671 (2020).

[57] M. Yu, D. R. Trinkle, Accurate and Efficient Algorithm for Bader Charge Integration, *J. Chem. Phys.* **134**, 064111 (2011).

[58] D. J. Griffiths, Introduction to Quantum Mechanics (Prentice Hall, Upper Saddle River, 1995), p. 141.

[59] F. J. Yang, Atomic Physics (Higher Education Press, Beijing, 2008), p. 134.

[60] J. Emsley, The Elements (Oxford University Press, Oxford, 1998), p. 244.

[61] Y. Yang, S. Meng and E. G. Wang, A Molecular Dynamics Study of Hydration and Dissolution of NaCl Nanocrystal in Liquid Water, *J. Phys.: Condens. Matter* **18**, 10165 (2006).

[62] Y. R. Luo, Experimental Data of Chemical Bond Energies (Science Press, Beijing, 2005), p. 4.

[63] M. Büttiker, R. Landauer, Traversal Time for Tunneling, *Phys. Rev. Lett.* **49**,

1739 (1982).

[64] Z. C. Wang, Thermodynamics • Statistical Physics (Higher Education Press, Beijing, 2000), 3rd Edition, p. 271-273.

[65] L. J. Lauhon, W. Ho. Direct Observation of the Quantum Tunneling of Single Hydrogen Atoms with a Scanning Tunneling Microscope. *Phys. Rev. Lett.* **85**, 4566 (2000).

[66] P. G. Sundell, G. Wahnström, Quantum Motion of Hydrogen on Cu(001) Using First-principles Calculations, *Phys. Rev. B* **70**, 081403(R) (2004).

[67] C. Z. Zheng, C. K. Yeung, M. M. Loy, X. Xiao. Quantum Diffusion of H on Pt(111): Step Effects. *Phys. Rev. Lett.* **97**, 166101 (2006).

[68] G. X. Cao, E. Nabighian, X. D. Zhu, Diffusion of Hydrogen on Ni(111) over a Wide Range of Temperature: Exploring Quantum Diffusion on Metals, *Phys. Rev. Lett.* **79**, 3696 (1997).

[69] R. P. Bell, The Tunnel Effect in Chemistry (Chapman and Hall, London, 1980).